Available online at www.sciencedirect.com

ScienceDirect

journal homepage: www.elsevier.com/locate/he

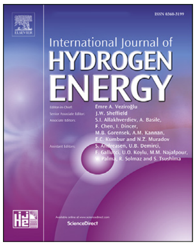

Large scale compatible fabrication of gold capped titanium dioxide nanoantennas using a shadowing effect for photoelectrochemical water splitting

T. Gamze Ulusoy Ghobadi [a,b,e,*], *Amir Ghobadi* [c,d], *Ferdi Karadas* [a,f], *Ekmel Ozbay* [a,c,d,g]

[a] *UNAM—National Nanotechnology Research Center, Bilkent University, Ankara, 06800, Turkey*
[b] *Institute of Materials Science and Nanotechnology, Bilkent University, Ankara, 06800, Turkey*
[c] *NANOTAM - Nanotechnology Research Center, Bilkent University, Ankara, 06800, Turkey*
[d] *Department of Electrical and Electronics Engineering, Bilkent University, Ankara, 06800, Turkey*
[e] *Department of Energy Engineering, Faculty of Engineering, Ankara University, Ankara, 06830, Turkey*
[f] *Department of Chemistry, Bilkent University, Ankara, 06800, Turkey*
[g] *Department of Physics, Bilkent University, Ankara, 06800, Turkey*

HIGHLIGHTS

- An elegant and large scale compatible plasmonic design is proposed.
- Near field effects and hot electron injection are main enhancement mechanisms.
- Excitation of multiple LSPR modes leads to a broad light harvesting.
- Proposed fabrication route is large scale compatible with no material restriction.
- Using visible responsive semiconductors, the enhancement can be more significant.

ARTICLE INFO

Article history:
Received 18 September 2019
Received in revised form
3 November 2019
Accepted 6 November 2019
Available online 7 December 2019

Keywords:
Plasmonics
Hot-electron
Water splitting
Photoelectrochemistry

ABSTRACT

In this paper, a visible light driven plasmonic based photoelectrochemical water splitting (PEC-WS) cell is designed with an elegant two-step fabrication route. First, titanium dioxide (TiO_2) nanowires (NWs) were synthesized using the hydrothermal method. Then, angled deposition was used to selectively coat the tips of the NWs yielding Au-capped TiO_2 NWs with multiple sizes and shapes. The provided randomness leads to a multi-resonant system where the superposition of these resonance modes leads to an overall broadband absorption. The excited localized surface resonance (LSPR) modes contribute to the performance enhancement of the cell via near field effects and a hot electron injection mechanism. Moreover, these nanotips can trigger the formation of Fabry-Pérot (FP) cavity modes. The combination of the above-mentioned mechanisms leads to a high performance visible light driven plasmonic cell. At an applied potential of 1.23 V vs RHE, a photocurrent value as high as 82 $\mu A/cm^2$ is acquired for the plasmonic based photoanode. The proposed design strategy is a large scale compatible route with no material restriction. Therefore, vast variety of semiconductor-metal pairs can be fabricated to obtain highly efficient water splitting cell for hydrogen generation.

---

* *Corresponding author*. UNAM—National Nanotechnology Research Center, Bilkent University, Ankara, 06800, Turkey.
E-mail address: gamze.ulusoy@bilkent.edu.tr (T.G. Ulusoy Ghobadi).

https://doi.org/10.1016/j.ijhydene.2019.11.060

Introduction

A major portion of the hydrogen generation comes from carbonaceous raw material, primarily fossil fuels. Just a fraction of this produced hydrogen is currently used for energy purposes; the rest serves as a chemical feedstock for petrochemical, food, electronics and metallurgical processing industries. However, hydrogen's use in the energy market is increasing with the implementation of fuel cell systems. The use of renewable resources for clean production of hydrogen holds a great promise. Among all, hydrogen generation using photoelectrochemical water splitting (PEC-WS) has attracted much attention in recent years. In this process, upon light illumination on the photoanode, electron and hole pairs are generated. Ideally, the electrons are transferred toward the cathode, via an external circuit under an applied bias voltage, where they produce H_2 gas. On the other side, the holes, at the photoanode, create O_2 by water oxidation.

Strong light-matter interaction in sub-wavelength geometries is the subject of many studies in recent years [1]. The use of proper materials in right configurations can lead to strong light absorption in broad or narrow frequency regimes. One of the most frequently employed components for the realization of light perfect absorption is metal [2]. Unlike semiconductors that can only absorb photons with energies above their optical band gap, metals keep their lossy nature throughout an ultrabroadband spectral range including the ultraviolet (UV), visible, and near infrared (NIR) regimes. Several recent studies have proven the ultra-broadband plasmonic light absorbers using lossy and noble metals [3–9]. Such broad light absorption will be of great interest for photoconversion applications. Plasmon-driven PEC-WS is one of these applications [10–14].

In these photoanodes, the localized surface plasmon resonances (LSPRs) are excited at the metal-semiconductor interface. LSPR can decay through two main pathways; (i) radiative, and (ii) non-radiative [11,12]. In radiative energy transfer, the semiconductor absorption is enhanced via near-field coupling or scattering. In fact, in this type of process, the plasmonic particle acts as a secondary source to improve the semiconductor absorption response. Therefore, these effects can only improve light absorption for photons with energies above the material band gap. In the non-radiative decay of LSPR, however, the photogenerated hot electrons are directly injected into the semiconductor conduction band. In other words, the plasmonic particle acts as a photoactive material and, therefore, a sub-band gap absorption can be achieved [15,16]. In the latter case, the absorption of light by metallic nanounits generates a large density of energetic electrons that are called hot electrons. The hot electrons that can pass the Schottky barrier (in metal-semiconductor interface) can contribute in photocurrent generation. These plasmonic-driven PEC-WS cells have been successfully realized in a variety of metal-semiconductor pairs [17–31]. One of the most common semiconductors for this architecture is titanium dioxide (TiO_2) due to its photocatalytic ability, chemical stability, earth abundance, and cost effectiveness [32–42]. However, it suffers from poor optical performance with an absorption tail in the UV range (λ < 400 nm). This absorption can be extended toward the visible regime by the incorporation of plasmonic particles where the excitation of visible light hot electrons and their injection into a semiconductor conduction band (CB) can tackle this drawback [43–50]. The use of different types of plasmonic particles such as Au [46], Ag [44,45,48], and Cu [47,49] has been demonstrated on TiO_2 nanostructures.

The chemically synthesized gold (Au) nanoparticles can be embedded into the bulk of the semiconductor [36,38] or on its surface [26,33,37,39]. The use of Au nanoparticles and nanorods on TiO_2 NWs for hot electron driven PEC-WS was demonstrated with photocurrent values as low as 10 $\mu A/cm^2$ and IPCE<0.015% [39]. The use of an interfacial layer [51] or a catalyst [52] can improve carrier's transport dynamics and this, in turn, increases the visible light driven IPCE. The utilization of iridium oxide between the Au and TiO_2 host leads to an IPCE of 0.6% [52]. However, besides the synthetic challenge of chemical approaches, they contain by-products that are not environmentally friendly. Therefore, the use of other innovative synthesis routes has attracted much attention in recent years. One of these approaches is dewetting [34,41,53,54]. In the dewetting process, a thin layer of metal is coated on the semiconductor surface and annealed at a temperature close to its melting point. The dewetting of Au thin film on a TiO_2 three dimensional Nanocone host was led to uniformly dispersed Au NPs, with IPCE values below 1% in the visible range [54]. However, this route contains a high temperature process and it can damage the semiconductor host. Moreover, in all of these methods, a large density of plasmonic nanounits are dispersed within the semiconductor volume. While these metallic nanoparticles enhance the light absorption of the cell, they also act as an electron trapping center that captures the carrier and diminishes their collection efficiency. That is why, at an optimum loading, they show performance improvement [25,27,53] and this in turn limits their repeatability. In addition, they have a material restriction and not all the metals can be synthesized by these approaches. Taking all the above discussion into consideration, the use of a large scale compatible architecture with a spatially selective coating of plasmonic metal can be proposed to obtain efficient plasmon-driven PEC-WS photoanode.

In this paper, inspired by our recent work [55], an elegant and large scale compatible design based on an Au-capped TiO_2 nanowires (NWs) antenna is proposed. In this configuration, densely packed, randomly oriented TiO_2 NWs are prepared using the hydrothermal method. Later, angled deposition is utilized to grow gold clusters on the tip of the NWs. Due to the shadowing effect of the NWs, their volume is not coated and only the top position is exposed to gold vapor. The radius of these Au caps is controlled with the NWs radius. Considering the randomness in the NWs geometries, different sized Au nanoislands are formed. These different sized particles can support LSPR modes in different wavelength values and the superposition of these resonance modes will lead to a broad light harvesting. The PEC characterizations show that the proposed structure can lead to an efficient visible-driven water splitting photoanode. The photocurrent value at 1.23 V vs RHE has been enhanced from 50 $\mu A/cm^2$ for the bare design to 82 μA/cm^2 for Au-capped photoanode. Our characterization results show that this enhancement originates from hot electron injection and near field effects of plasmonic Au nanocaps. The near field effects lead to better charge generation and separation in the semiconductor layer while the hot electron injection provides photocurrents in the visible regimes (up to 480 nm). Due to its large scale compatibility and lack of material restriction, it is envisioned that the proposed strategy can be used to realize efficient plasmon-driven photoconversion devices. The photocurrent enhancement can be much more significant, if we use a visible responsive semiconductor as NW, where the formation of FP modes can significantly enhance light-matter interaction within the semiconductor bulk as well.

Materials and methods

Materials

All of the chemicals were used as received without further purification. Titanium (IV) butoxide ($Ti(OBu)_4$, 97%, Sigma–Aldrich), hydrochloric acid (HCl, 36%, Sigma–Aldrich), and Millipore deionized water (resistivity: 18 mΩ cm) was used for the hydrothermal growth of TiO_2 NWs on FTO coated glass (2 mm thick, 7 Ω sq-1, Solaronix).

Synthesis of Au-capped TiO_2 nanowires

TiO_2 NW arrays were synthesized by modifying the hydrothermal technique as described in our previous studies [56–58]. In detail, 1 mL of $Ti(OBu)_4$ was added dropwise to the HCl solution (accompanied by intense stirring), which was prepared with the volume ratio of concentrated HCl to deionized (DI) water being 1:1. After being stirred for 30 min, under ambient conditions, the precursor solution was transferred to a Teflon-lined stainless steel autoclave (capacity of 45 mL) with an FTO conducting side facing up with 60° angle against the wall. In advance, FTO glasses (1 cm × 2 cm) were cleaned sufficiently in sonication baths in DI water, acetone, and ethanol in sequence, each for 15 min and then dried by N_2 flow. The hydrothermal reaction was carried out at 180 °C for 3 h, and then it is allowed to cool down at room temperature. After cooling, the substrate was thoroughly rinsed in deionized water. Following growth, the substrate was annealed in a tube furnace in air at 450 °C for 2 h. Later, using the angled deposition technique, 20 nm gold was evaporated on the sample to form an Au-capped TiO_2 NW sample.

Characterizations

Materials characterization

The morphological characteristics of the synthesized photoanode materials were performed using a scanning electron microscope (SEM, FEI – Quanta 200 FEG) operated at 10 kV. A transmission electron microscope (TEM, Tecnai G2-F30, FEI) was operated at 200 kV. TEM samples were dispersed in ethanol and prepared on a holey carbon coated copper grid. X-ray photoelectron spectroscopy (XPS, Thermoscientic K-Alpha, Al K-Alpha radiation, hυ = 1486.6 eV) measurement was performed in survey mode by operating a flood gun to prevent surface charging with the pass energy and step size set to 30 eV and 0.1 eV, respectively. Peak positions correction was calibrated by referencing the C1s peak position (284.8 eV) and shifting other peaks in the spectrum accordingly. For the optical characterization of the NWs, a UV-Vis-NIR spectrophotometer (Cary 5000, Varian) was employed.

Photoelectrochemical measurements

(Photo)electrochemical measurements were performed using a Gamry Instruments Interface 1000 Potentiostat/Galvanostat in a standard three-electrode electrochemical cell configuration with bare TiO_2 NWs and Au capped-TiO_2 NWs with an exposed area of 1 cm^2, Pt mesh, and Ag|AgCl|KCl(sat) as the working, counter, and reference electrodes, respectively. All of the calculations were based on the geometric surface area, unless specified. The measurements on photoanodes have been performed in phosphate-buffered saline (0.5 M Na_2SO_4 in 0.1 M PBS, pH 7 at 25 °C) and, prior to each measurement, the electrolyte solution was saturated with N_2 gas (99.999% purity) for 30 min to remove the dissolved O_2 gas. The solar light simulator (Sciencetech, Model SLB-300B, 300 W Xe lamp, AM 1.5 global filter) was calibrated to 1 sun (100 mW/cm2) using a thermopile optical detector (Newport, Model 818P-010-12).

The current density–voltage (j–V) curves were measured on photoanodes in 0.1 M PBS under dark and light conditions with a scanning rate of 50 mV/s between −0.4 and 1.3 V (vs Ag/AgCl) by the Linear sweep voltammetry (LSV) measurements. Transient photocurrent measurements by the chronoamperometry (CA) technique, electrochemical impedance spectroscopy (EIS) under light condition, and open-circuit voltage decay (OCVD) were also conducted in the same system. EIS spectra were recorded in the frequency range from 10 kHz to 0.1 Hz at a bias of 1.23 V vs RHE with an alternating current (AC) voltage of 10 mV. Mott-Schottky measurements were performed at potentials varying between −0.7 and 0.5 V (vs Ag/AgCl) to extract electrodes donor densities (N_d) and flat band potentials (V_{fb}), where the frequency is set at 5 KHz.

For incident photon-to-current conversion efficiency (IPCE) measurement, light from the xenon lamp was dispersed by a monochromator and the photocurrent was recorded at a constant bias (1.23 V vs RHE) with a spectral step of 10 nm. This light is entered into a monochromator (Oriel 1/8 m cornerstone, 1200 lines/mm grating) and the output of the monochromator is illuminated onto the sample.

Results and discussion

Fig. 1a schematically represents the fabrication setup of our Au-capped TiO_2 NWs. In this fabrication route, the sample is placed in a near vertical orientation (with an approximate angle of $\Theta > 80°$) in the thermal evaporation tool. The mechanism responsible for the creation of gold nanocaps is depicted in Fig. 1b. As shown in this panel, the formation of these nanoislands are promoted via the shadowing effect of the NWs. The diameter of these gold tips is controlled with the NWs diameter. The resultant plasmonic Au-capped TiO_2 NW sample is schematically shown in Fig. 1c. To verify the experimental results of this process, SEM images of the

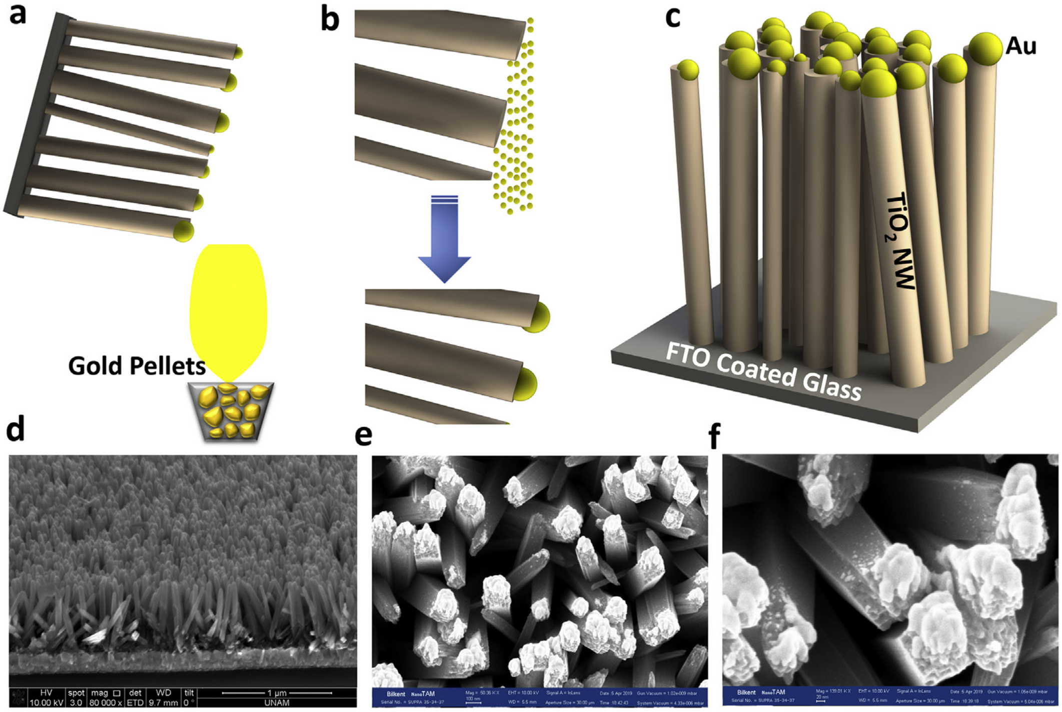

Fig. 1 – Schematic representation of fabrication route for Au-capped TiO_2 on FTO substrates: (a) Angled Au deposition on hydrothermally grown TiO_2 NWs by thermal evaporator, (b) the mechanism responsible for formation of Au nanoparticles on top of the substrate due to shadowing effect of the NWs. (c) Architecture of the obtained Au-capped TiO_2 photoanode sample at the end of process. (d) Cross sectional, (e) Top, and (f) high-magnification SEM images of Au-capped TiO_2 photoanode.

sample have been acquired, as depicted in Fig. 1d–f. From Fig. 1d, the obtained NWs have an average length of 0.5 μm. As these panels imply, the hydrothermally grown TiO_2 NWs have random diameter and orientation. This randomness leads to formation of multiple sized gold nanocaps. Moreover, the shape of these islands is influenced by NWs orientation, see Fig. 1f. Therefore, the proposed preparation strategy provides a facial approach to synthesize plasmonic photoanode for PEC-WS. In the following sections, we will scrutinize the photoelectrochemical activity of these plasmonic samples.

To begin with, the effect of Au capping on the PEC performance of TiO_2 NW arrays is investigated in a three-electrode configured cell. Linear-sweep voltammograms (LSVs) of TiO_2 NWs and Au-capped TiO_2 photoanodes under chopped visible light illumination (($\lambda > 420$ nm) are illustrated in Fig. 2a. Stabilized photocurrent densities were measured after third scan with continuous illumination for all of the photoanodes. In a typical measurement, 420 nm cut-off filter is used to determine whether the measured photocurrent was associated with the hot electron injection of Au, indicating that pristine TiO_2 nanoarray electrode has no response in the visible light region. Indeed, there is an overlap between TiO_2 absorption tail and cut-off edge of the filter, there seems to be still some current in this spectral region, which will further be discussed in the upcoming parts. As can be clearly seen in Fig. 2a, the incorporation of an Au cap on top of TiO_2 NW has significantly improved its photocurrent response. At an applied potential of 0.62 V vs Ag/AgCl (corresponded to 1.23 V vs RHE), the photocurrent densities of the bare TiO_2 NWs and Au-capped TiO_2 NW samples are recorded to be 50 μA/cm^2 and 82 μA/cm^2, respectively. Moreover, the long-term stability as a function of irradiation time for Au-capped and bare TiO_2 photoanodes have been investigated using a transient-current measurement (chronoamperometry) at 0.2 V vs Ag/AgCl, Fig. 2b. As clearly visualized, the photocurrent density is almost constant during 2 h of illumination, which verifies that the photoanode maintains its original structure throughout the experiment. From these CA spectra, the amount of evolved hydrogen is extracted from the charge passed during bulk electrolysis for 2 h duration. This data has been shown in Fig. 2c. The significant enhancement in the photocurrent of TiO_2 NWs has been acquired by just exposing Au nanoparticles on top of NWs rather than their whole surface. It is speculated that this improvement mainly originates from the localized surface plasmon resonance (LSPR) effect of Au NPs. As already explained, LSPR can decay through two main pathways; (i) radiatively, and (ii) non-radiatively. In radiative energy, transfer, the semiconductor absorption is enhanced via near-field coupling or scattering. In fact, in this type of process, the plasmonic particle acts as a secondary source to improve the semiconductor absorption response. In the non-radiative decay of LSPR, however, the photogenerated hot electrons are directly injected into semiconductor conduction band. In other words, the plasmonic particle acts as a photoactive material. The densely packed randomly oriented NWs have a high scattering cross section deduced from their white color as shown in the inset of Fig. 2a. In other words, the bare photoanode is a high performance trapping scaffold.

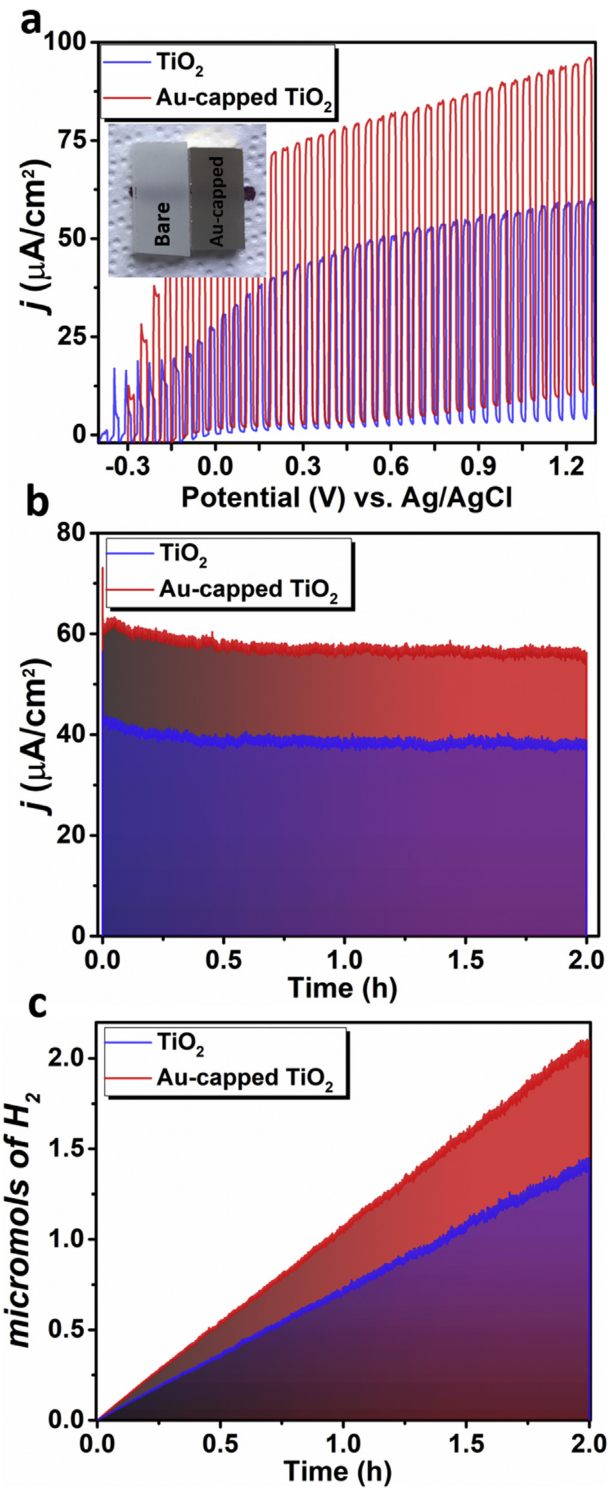

Fig. 2 – The bare TiO_2 NWs, and Au-capped TiO_2 NWs: (a) j-V LSV plots by chopped visible light illumination ($\lambda > 420$ nm), (b) j-t plots under solar irradiation for 2 h at 0.2 V (vs Ag/AgCl), and (c) the amount of evolved hydrogen extracted from the charge passed during bulk electrolysis for 2 h. The inset shows the fabricated bare and Au-capped samples. Measurements are conducted in N_2-saturated 0.5 M PBS (pH 7) electrolyte.

Therefore, it is envisioned that the scattering by Au caps can be eliminated or has a minor contribution to our PEC performance improvement. In fact, the structure by itself can absorb most of above band gap photons. This scaffold also has high scattering in the visible spectrum where the TiO_2 NWs are inactive. Therefore, an elegant integration of visible responsive materials into this.

Trapping host can lead to an efficient visible responsive photoanode. The nano gold assembly can take this responsibility. The dark appearance of the plasmonic sample proves this fact (inset of Fig. 2a). The Au nanocap will absorb the visible spectrum of the electromagnetic wave and the excited hot electrons (with enough energy to pass the Schottky barrier) are injected into TiO_2 conduction band (CB). Based on these discussions, it is speculated that the dominant plasmonic energy transfer mechanism is most likely to be the hot-electron injection from Au to CB of TiO_2, in our proposed plasmonic design. To verify our assumption, the samples are characterized from three main perspectives: (i) structural, (ii) optical, and (iii) electrical properties. Since the electron transport layer is TiO_2, its crystallinity has utmost importance in the efficient collection of photo carriers. Fig. 3a shows an HRTEM image of the individual TiO_2 NWs, indicating the good crystallinity of the materials. It should be noted that TiO_2 NWs prepared by this hydrothermal method can be single crystalline with the rutile phase, which has been reported previously [59]. Moreover, the phase structure of TiO_2 is determined by XRD patterns as shown in Fig. 3b. All the peaks are in agreement with the standard diffraction pattern of rutile TiO_2 (JCPDS, 82–0514), with the prominent (110) rutile phase. Furthermore, to determine the specific surface composition and chemical state of the Au-capped TiO_2 and bare TiO_2 NWs, XPS measurement is employed. The 1/2 and 3/2 spin-orbit doublet components of the Ti^{4+} and Ti2p spectrum of TiO_2 sample are located at 463.44 eV and 457.77 eV, respectively (see Fig. 3c). After Au NPs deposition, Ti 2p peaks shift to higher binding energies (~0.6 eV) at 464.11 eV and 458.46 eV verifying the electron transfer between Au and TiO_2 [33] (see Fig. 3d). Moreover, Fig. 3e displays the Au4f XPS spectra of Au-capped TiO_2. The binding energies at 86.92 eV and 83.24 eV are ascribed to Au $4f_{5/2}$ and Au $4f_{7/2}$, respectively [35]. According to this figure, Au 4f7/2 peak exhibits a negative shift (~0.8 eV) compared to bulk metallic gold Au° ($4f_{7/2}$ at 84 eV), which can be due to the electron transfer from oxygen vacancies to Au, leading to a lower binding energy of Au $4f_{7/2}$ and a higher one of Ti2p in Au-capped TiO_2 NWs [33].

The light absorption performance of photoanodes was assessed with absorption spectroscopy studies. As shown in Fig. 3f, after the deposition of Au on top of the TiO_2 NWs, the Au-embedded TiO_2 electrode shows a reduced transmission in the visible light range. From this, it can be concluded that absorption has been improved in the plasmonic photoanode. It is well-known that TiO_2 has no absorbance in the visible spectrum and, therefore, this absorption stems from the plasmonic response of Au capping. To address this broad absorption response, the numerical simulations, using a commercial finite-difference time-domain (FDTD) software package (Lumerical FDTD Solutions) [60] are conducted Fig. 4a shows the unit cell used in our simulation. The periodicity of the unit cell is set as 150 nm, the length of nanowire is fixed at

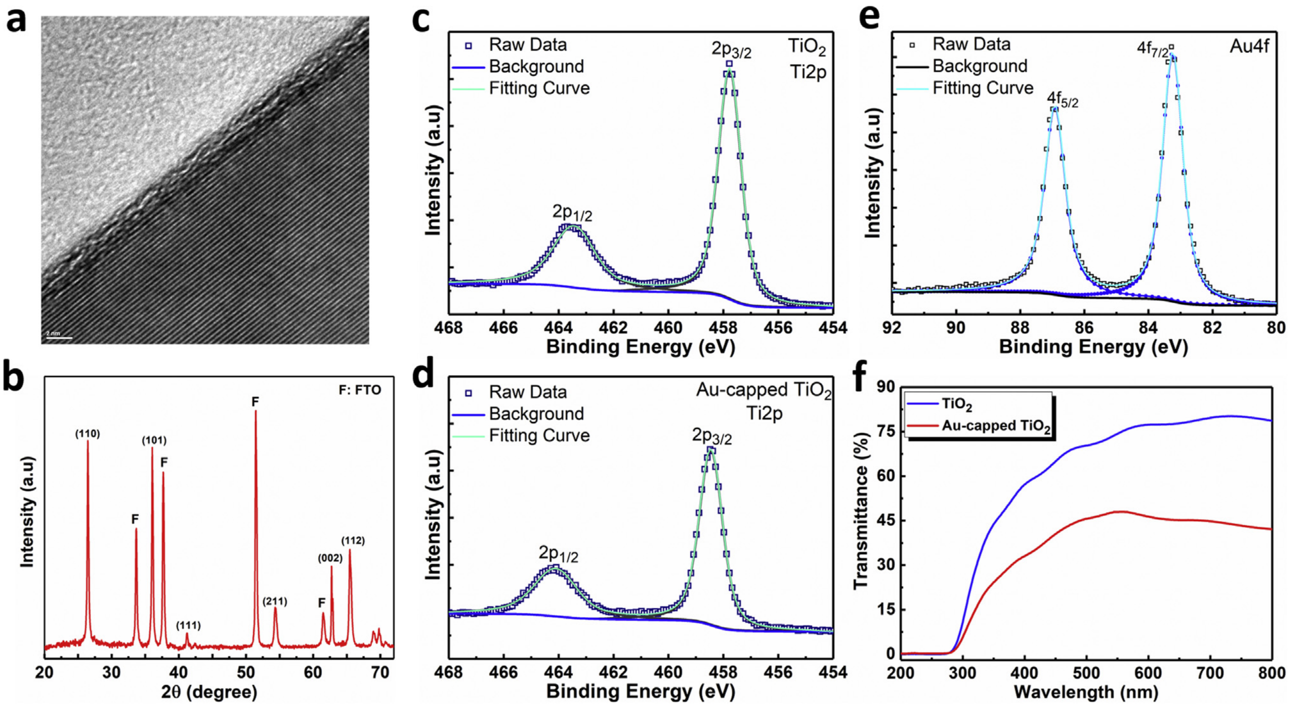

Fig. 3 – The bare TiO_2 NWs (a) HR-TEM image, (b) XRD patterns with diffraction patterns, (c) High resolution XPS spectra of Ti2p for bare TiO_2 NW sample, (d) Ti2p and (e) Au4f spectra for the Au-capped TiO_2 samples, and (f) the transmittance profiles for both samples at a wavelength range of 200 nm–800 nm.

0.5 μm, the thickness of gold cap is chosen as 20 nm. Fixing these geometries, a sweep is conducted to.

Understand the effect of gold cap width on the absorption profile of the design. The boundary conditions in the lateral directions (x and y) are set as periodic and in the z direction the perfectly matched layer (PML) condition is chosen. It should be noted that the real device is a non-periodic pattern but our goal in these simulations is to find the impact of gold capping on the absorption response of the system. Fig. 4b shows the amount of normalized absorbed power within the

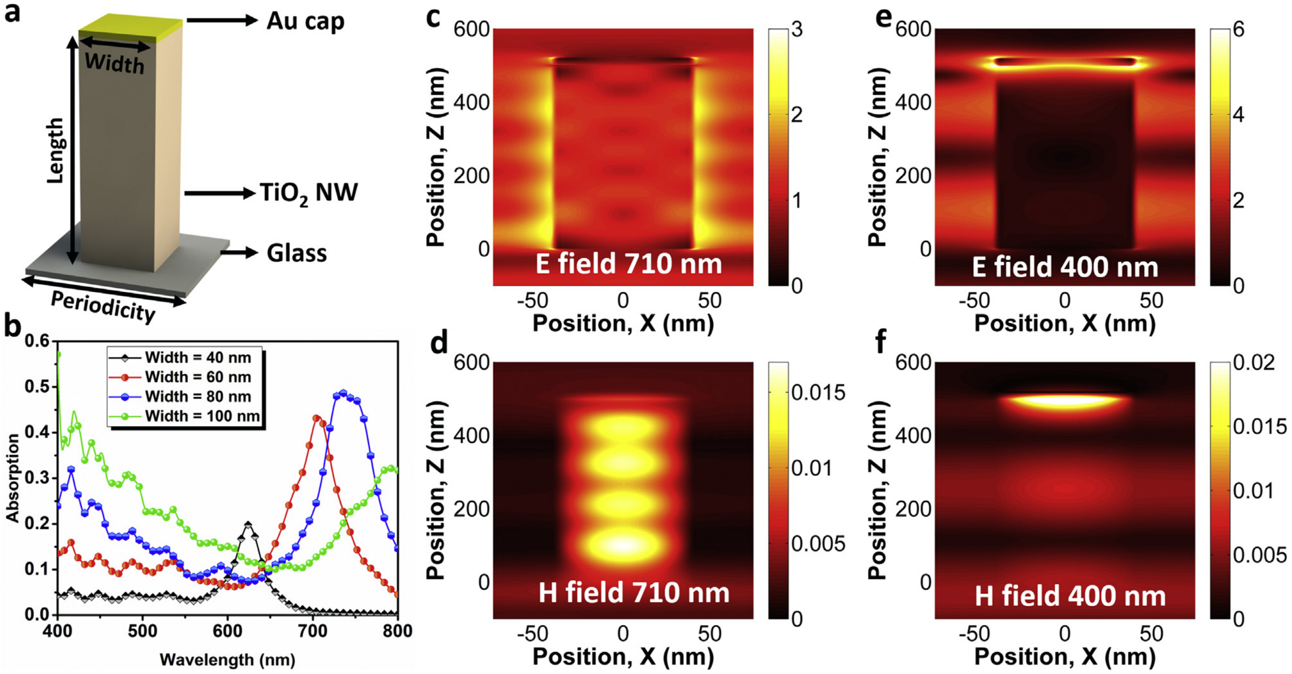

Fig. 4 – (a) The simulation unit cell, (b) The normalized absorption as a function of cap width. (c) The E-field and H-field distribution across the design at (c–d) 710 nm, and (e–f) 400 nm.

Au cap, as a function of the cap width. As the width increases, absorption profiles show a red-shift in the visible region. Moreover, each specific width has a relatively narrow absorption peak at a certain wavelength. Considering the fact that the synthesized NW arrays have random geometries (various width, length and orientation), the structure has multiple resonances and the superposition of them leads to a flat and broad absorption response. To understand the nature of this absorption, electric and magnetic field profiles have been extracted in on-resonance (710 nm) and off-resonance (400 nm) conditions, Fig. 4c–f. As these panels describe, the gold cap excites Fabry-Perot (FP) modes in the cavity. In the resonance frequency, the magnetic and electric fields are confined in the gold tip and this field localization leads to strong light absorption in the gold layer. In fact, the structure acts as a lossy antenna that confine light and harvest it in an efficient way.

Based on above discussions, the proposed sample has superior optical properties. Another factor that defines the activity of a PEC-WS cell is its carrier dynamics. Therefore, we further probed the interfacial properties between the photoelectrode and the electrolyte. To determine the effect of the Au-capping on the carrier density of the TiO_2 NWs, Mott-Schottky measurement was performed. The measurement has been conducted at a high frequency of 5 KHz to ensure that the contribution of surface state capacitance can be safely neglected. The carrier concentration can be estimated using the below Mott–Schottky relation, where C_{SC} is the space charge capacity, e is the charge of an electron, ε_0 is the vacuum permittivity, ε_r is the relative permittivity (dielectric constant) of the sample, A is the electrochemically active surface area, N_d is the majority charge carrier (donor) density, $V_{Applied}$ is the applied voltage (vs. Ag/AgCl), V_{fb} is the flat band potential, k_B is the Boltzmann constant, and T is the absolute temperature.

$$\frac{1}{C_{SC}{}^2}=\frac{2}{(\varepsilon_r\varepsilon_o A^2 e N_d)}\times\left(V_{Applied}-V_{fb}-\frac{k_B T}{e}\right) \tag{1}$$

From the slopes of the Mott Schottky plots (Fig. 5a), Au-capped TiO_2 NWs exhibit slightly smaller slopes compared to pristine sample, suggesting their larger conductivity. Mott-Schottky plot is derived from a flat electrode model, thereby determining the absolute value of A in such dense nanowire arrays is not a straightforward task. However, the ratio between slopes inversely corresponds to the ratio of N_ds. It is clear that the higher N_d of Au-embedded TiO_2 NWs implied a lower resistance and faster carrier transfer than bare TiO_2 NWs, and so an enhanced PEC performance. Based on the profiles obtained in Fig. 5a, the V_{fb}s are also extracted from the intercept extrapolating a straight line from $1/C^2$ versus.

Potential plot as −0.55 V and −0.54 V (vs Ag/AgCl) for TiO_2 NWs, and Au-capped TiO_2 NWs, respectively. In addition, both samples show positive slopes in Mott-Schottky plots, as expected for n-type semiconductors. These results are further confirmed by conducting electrochemical impedance spectroscopy (EIS), which is a powerful tool to clarify the transport resistance in PEC-WS system. Fig. 5b illustrates the Nyquist plot of EIS in a frequency range of 0.1 Hz–10 KHz using an AC amplitude of 10 mV, at an applied potential of 0.62 V vs Ag/AgCl under visible light illumination ($\lambda > 420$ nm) so that the carrier generation and separation kinetics during the oxygen evolution reaction could be evaluated. Based on previous findings, the incorporation of plasmonics has significantly improved the optical response and carrier concentration. However, besides this effect, Au nanocap can also enhance the carrier separation in metal-semiconductor interface. The formation of the Schottky junction at the metal-semiconductor contact leads to a space charge region in the semiconductor side. This consequently causes a better charge carrier separation dynamic. This can be observed from the Nyquist plot of EIS. In this plot, a semicircle at low frequencies refers to the charge-transfer process in the PEC system, and the diameter of the semicircle represents the charge-transfer resistance (R_{ct}) (resistivity in the depletion region) at the semiconductor/electrolyte junction [25]. Clearly, the semicircle diameter of Au-embedded TiO_2 NWs under photoirradiation are smaller than that of TiO_2 NWs, indicating their lower resistance. This further confirms the Mott Schottky results.

In order to evaluate the carrier lifetimes of the NW arrays and interfacial charge transfer process, OCVD measurement is performed. Fig. 5c shows the exponential decays of the photovoltage after turning off the illumination. The samples are illuminated for ~20 s to obtain a steady open-circuit voltage (V_{oc}), and then the illumination was turned off using a shutter, and the V_{OC} decay is recorded under dark. Once light is terminated, the V_{OC} returns to its initial value in the dark condition via the recombination of photogenerated carriers. According to Fig. 5c, the decay dynamics for both samples are quite similar with a slightly longer lifetime for the Au-capped sample. Indeed, to change the electron decay rates and collect the information about recombination mechanisms like (i) band-to-band transition, and (ii) band to surface transition, there should be structural or surface change within the volume. However, in our case, Au cannot change the either TiO_2 bulk or its surface. This is the reason why both samples have the same V_{oc} decay. Another feature that can be highlighted in this experimental result is the photovoltage value. The photovoltage is defined as the difference between open circuit potentials in the dark, and under illumination conditions. For the Au-capped plasmonic sample this difference is larger compared to that of pristine one. This stems from the ability of Au nanounits to generate hot carriers. In other words, this enhanced photovoltage shows the generation larger carrier concentration in the plasmonic sample. All of the photoelectrochemical measurements discussed above suggest an enhancement in the photoactivity of the plasmonic sample, in comparison with the bare sample. However, the responsible mechanism cannot be truly assessed based on these data. In.

Other words, it is not possible to distinguish which portions of this improvement are attributed to near field effects and hot electron injection. To have a better understanding on this issue, we have synthesized a thin TiO_2 NW sample with a hydrothermal growth duration of 1 h. The inset of Fig. 5d shows the optical image of bare and plasmonic samples. The pulsed CA is utilized to measure dark and light responses of the samples, at an applied bias of 1.23 V vs RHE. As shown in Fig. 5d, the pristine sample (1 h TiO_2 NW) has no response upon solar light irradiation. However, the Au-capped photoanode shows a ~12 $\mu A/cm^2$ current difference between dark

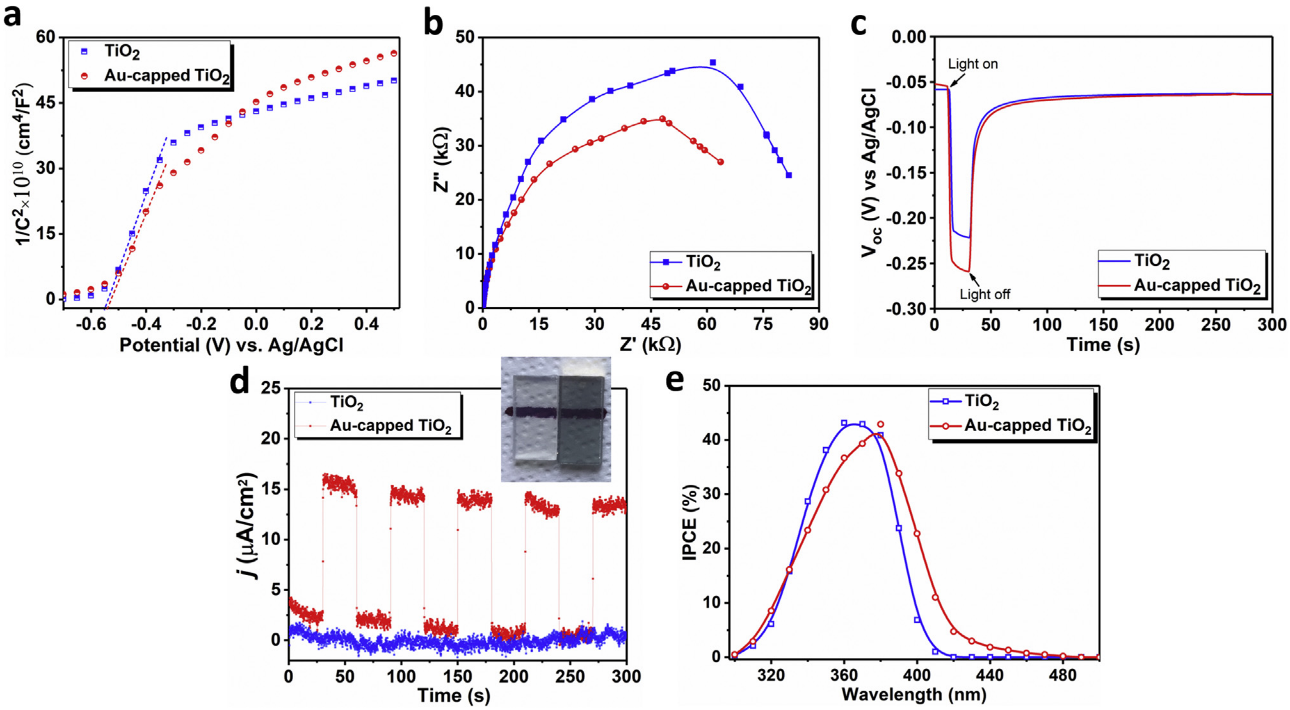

Fig. 5 – The bare TiO_2 NWs, and Au-capped TiO_2 NWs: (a) The Mott-Schottky profiles under dark (b) EIS Nyquist plots at a bias of 0.2 V (vs. open circuit), in the frequency range 1 Hz to 0.1 kHz under visible light irradiation ($\lambda > 420$ nm), (c) OCVD measurement as a function of time, (d) The pulsed CA results for 1 h grown bare and Au-capped TiO_2 NWs, and (e) IPCE values in a wavelength range of 300 nm–500 nm.

and light conditions. A better qualitative comparison can be acquired by measuring the incident photon conversion efficiency (IPCE) values of the samples. As depicted in Fig. 5e, the IPCE response of the bare NW sample goes to zero at a wavelength of 420 nm. However, the IPCE response for Au-capped TiO_2 NW sample is extended up to 480 nm. Considering the large optical band gap of TiO_2, this sub band gap visible light response is attributed to hot electron injection from excited states of nanogold into CB of TiO_2. Therefore, it can be concluded that the photocurrent response of the Au-capped TiO_2 NW sample is a combination of near field enhancement effects and hot electron injection.

Conclusion

In this study, we have developed a facial, and large scale compatible approach to fabricate plasmonic hot electron driven PEC-WS cell. The proposed structure shows a superior optical response with a broadband absorption in the visible part of the spectrum. The nature of this broadband absorption response was investigated using FDTD simulations. Later, the PEC measurement results demonstrated that this enhanced photoresponse is attributed to both near field effects and hot electron injection. The IPCE measurement proved a photoconversion efficiency of up to 480 nm. This visible responsive plasmonic photoanode has a photocurrent value as high as 82 μA/cm². The findings of this paper can be employed to design robust and efficient plasmonic photoconversion devices.

Acknowledgements

This work is supported by the Scientific and Technological Research Council of Turkey (TUBITAK), grant number 215Z249. This work is supported by the project DPT-HAMIT as well as TUBITAK under the project nos. 113E331, 114E374, and 115F560. One of the authors (E.O.) also acknowledges partial support from the Turkish Academy of Sciences.

REFERENCES

[1] Ghobadi A, Hajian H, Butun B, Ozbay E. Strong light – matter interaction in lithography-free planar metamaterial perfect absorbers. ACS Photonics 2018;5:4203–21. https://doi.org/10.1021/acsphotonics.8b00872.

[2] Li Z, Butun S, Aydin K. Large-area, Lithography-free super absorbers and color filters at visible frequencies using ultrathin metallic films. ACS Photonics 2015;2:183–8. https://doi.org/10.1021/ph500410u.

[3] Li Z, Butun S, Aydin K. Large-area, Lithography-free super absorbers and color filters at visible frequencies using ultrathin metallic films. ACS Photonics 2015;2:183–8. https://doi.org/10.1021/ph500410u.

[4] Ghobadi A, Hajian H, Rashed AR, Butun B, Ozbay E. Tuning the metal filling fraction in absorbers to maximize the absorption bandwidth. Photonics Reseach 2018;6:168–76.

[5] Ghobadi A, Hajian H, Dereshgi SA, Bozok B, Butun B, Ozbay E. Disordered nanohole patterns in metal-insulator multilayer for ultra-broadband light absorption: Atomic layer deposition for lithography free highly repeatable large scale multilayer growth. Sci Rep 2017;7:1–10. https://doi.org/10.1038/s41598-017-15312-w.

[6] Ji C, Lee K, Xu T, Zhou J, Park HJ, Guo LJ. Engineering light at the Nanoscale : structural color filters and broadband perfect absorbers. Adv. Opt. Mater. 2017;5:1700368. https://doi.org/10.1002/adom.201700368.

[7] Ghobadi A, Hajian H, Gokbayrak M, Dereshgi SA, Toprak A, Butun B, Ozbay E. Visible light nearly perfect absorber: an optimum unit cell arrangement for near absolute polarization insensitivity. Opt Express 2017;25:27624. https://doi.org/10.1364/OE.25.027624.

[8] Ghobadi A, Hajian H, Gokbayrak M, Butun B, Ozbay E. Bismuth-based metamaterials: from narrowband reflective color filter to extremely broadband near perfect absorber. Nanophotonics 2019;8:823–32. https://doi.org/10.1515/nanoph-2018-0217.

[9] Ghobadi A, Hajian H, Soydan MC, Butun B, Ozbay E. Lithography-Free planar band-pass reflective color filter using series connection of cavities. Sci Rep 2019;9:1–11.

[10] Ghobadi TGU, Ghobadi A, Ozbay E, Karadas F. Strategies for plasmonic hot-electron-driven photoelectrochemical water splitting. ChemPhotoChem 2018;2:1–23. https://doi.org/10.1002/cptc.201700165.

[11] Hou W, Cronin SB. A review of surface plasmon resonance-enhanced photocatalysis. Adv Funct Mater 2013;23:1612–9. https://doi.org/10.1002/adfm.201202148.

[12] Brown AM, Sundararaman R, Narang P, Goddard WA, Atwater HA. Nonradiative plasmon decay and hot carrier dynamics: effects of phonons, surfaces, and geometry. ACS Nano 2016;10:957–66. https://doi.org/10.1021/acsnano.5b06199.

[13] Liu G, Du K, Xu J, Chen G, Gu M, Yang C, Wang K, Jakobsen H. Plasmon-dominated photoelectrodes for solar water splitting. J Mater Chem A 2017;5:4233–53. https://doi.org/10.1039/c6ta10471a.

[14] Ghobadi A, Ulusoy Ghobadi TG, Karadas F, Ozbay E. Semiconductor thin film based metasurfaces and metamaterials for photovoltaic and photoelectrochemical water splitting applications. Adv. Opt. Mater. 2019;1900028:1900028. https://doi.org/10.1002/adom.201900028.

[15] Lee J, Mubeen S, Ji X, Stucky GD, Moskovits M. Plasmonic photoanodes for solar water splitting with visible light. Nano Lett 2012;12:5014–9. https://doi.org/10.1021/nl302796f.

[16] Kodiyath R, Manikandan M, Liu L, V Ramesh G, Koyasu S, Miyauchi M, Sakuma Y, Tanabe T, Gunji T, Duy Dao T, Ueda S, Nagao T, Ye J, Abe H. Visible-light photodecomposition of acetaldehyde by TiO2-coated gold nanocages: plasmon-mediated hot electron transport via defect states. Chem Commun 2014;50:15553–6. https://doi.org/10.1039/c4cc06229a.

[17] Basheer AA, Ali I. Water photo splitting for green hydrogen energy by green nanoparticles. Int J Hydrogen Energy 2019;44:11564–73. https://doi.org/10.1016/j.ijhydene.2019.03.040.

[18] Huang Y, Liu J, Cao D, Liu Z, Ren K, Liu K, Tang A, Wang Z, Li L, Qu S, Wang Z. Separation of hot electrons and holes in Au/LaFeO3 to boost the photocatalytic activities both for water reduction and oxidation. Int J Hydrogen Energy 2019;44:13242–52. https://doi.org/10.1016/j.ijhydene.2019.03.182.

[19] Kumar D, Singh S, Khare N. Plasmonic Ag nanoparticles decorated NaNbO3 nanorods for efficient photoelectrochemical water splitting. Int J Hydrogen Energy 2018;43:8198–205. https://doi.org/10.1016/j.ijhydene.2018.03.075.

[20] Sharma S, Kumar D, Khare N. Plasmonic Ag nanoparticles decorated Bi 2 S 3 nanorods and nanoflowers: their comparative assessment for photoelectrochemical water splitting. Int J Hydrogen Energy 2019;44:3538–52. https://doi.org/10.1016/j.ijhydene.2018.11.238.

[21] Lan Y, Liu Z, Liu G, Guo Z, Ruan M, Rong H, Li X. 1D ZnFe2O4 nanorods coupled with plasmonic Ag, Ag2S nanoparticles and Co-Pi cocatalysts for efficient photoelectrochemical water splitting. Int J Hydrogen Energy 2019;44:19841–54. https://doi.org/10.1016/j.ijhydene.2019.05.184.

[22] Reddy NL, Rao VN, Vijayakumar M, Santhosh R, Anandan S, Karthik M, Shankar MV, Reddy KR, Shetti NP, Nadagouda MN, Aminabhavi TM. A review on frontiers in plasmonic nano-photocatalysts for hydrogen production. Int J Hydrogen Energy 2019;44:10453–72. https://doi.org/10.1016/j.ijhydene.2019.02.120.

[23] Pawar GS, Elikkottil A, Pesala B, Tahir AA, Mallick TK. Plasmonic nickel nanoparticles decorated on to LaFeO 3 photocathode for enhanced solar hydrogen generation. Int J Hydrogen Energy 2019;44:578–86. https://doi.org/10.1016/j.ijhydene.2018.10.240.

[24] Qin L, Wang G, Tan Y. Plasmonic Pt nanoparticles—TiO2 hierarchical nano-architecture as a visible light photocatalyst for water splitting. Sci Rep 2018;8:1–13. https://doi.org/10.1038/s41598-018-33795-z.

[25] Jeong SY, Shin HM, Jo YR, Kim YJ, Kim S, Lee WJ, Lee GJ, Song J, Moon BJ, Seo S, An H, Lee SH, Song YM, Kim BJ, Yoon MH, Lee S. Plasmonic silver nanoparticle-impregnated nanocomposite BiVO4 photoanode for plasmon-enhanced photocatalytic water splitting. J Phys Chem C 2018;122:7088–93. https://doi.org/10.1021/acs.jpcc.8b00220.

[26] Zhang X, Liu Y, Kang Z. 3D branched ZnO nanowire arrays decorated with plasmonic Au nanoparticles for high-performance photoelectrochemical water splitting. ACS Appl Mater Interfaces 2014;6:4480–9. https://doi.org/10.1021/am500234v.

[27] Kushwaha A, Aslam M. Defect controlled water splitting characteristics of gold nanoparticle functionalized ZnO nanowire films. RSC Adv 2014;4:20955–63. https://doi.org/10.1039/c4ra00782d.

[28] Li C, Wang P, Li H, Wang M, Zhang J, Qi G, Jin Y. Plasmon-driven water splitting enhancement on plasmonic metal-insulator-semiconductor hetero-nanostructures: unraveling the crucial role of interfacial engineering. Nanoscale 2018;10:14290–7. https://doi.org/10.1039/c8nr03557a.

[29] Kim S, Yu Y, Jeong SY, Lee MG, Jeong HW, Kwon YM, Baik JM, Park H, Jang HW, Lee S. Plasmonic gold nanoparticle-decorated BiVO 4/ZnO nanowire heterostructure photoanodes for efficient water oxidation. Catal. Sci. Technol. 2018;8:3759–66. https://doi.org/10.1039/c8cy00685g.

[30] Zwara J, Paszkiewicz-Gawron M, Łuczak J, Pancielejko A, Lisowski W, Trykowski G, Zaleska-Medynska A, Grabowska E. The effect of imidazolium ionic liquid on the morphology of Pt nanoparticles deposited on the surface of SrTiO3 and photoactivity of Pt–SrTiO3 composite in the H2 generation reaction. Int J Hydrogen Energy 2019;44:26308–21. https://doi.org/10.1016/j.ijhydene.2019.08.094.

[31] Subramanyam P, Khan T, Neeraja Sinha G, Suryakala D, Subrahmanyam C. Plasmonic Bi nanoparticle decorated BiVO4/rGO as an efficient photoanode for photoelectrochemical water splitting. Int J Hydrogen Energy 2019. https://doi.org/10.1016/j.ijhydene.2019.08.214.

[32] Wu M, Chen WJ, Shen YH, Huang FZ, Li CH, Li SK. In situ growth of matchlike ZnO/Au plasmonic heterostructure for enhanced photoelectrochemical water splitting. ACS Appl Mater Interfaces 2014;6:15052–60. https://doi.org/10.1021/am503044f.

[33] Su F, Wang T, Lv R, Zhang J, Zhang P, Lu J, Gong J. Dendritic Au/TiO2 nanorod arrays for visible-light driven photoelectrochemical water splitting. Nanoscale 2013;5:9001–9. https://doi.org/10.1039/c3nr02766j.

[34] Yen YC, Chen JA, Ou S, Chen YS, Lin KJ. Plasmon-enhanced photocurrent using gold nanoparticles on a three-dimensional TiO2 nanowire-web electrode. Sci Rep 2017;7:1–8. https://doi.org/10.1038/srep42524.

[35] Shiraishi Y, Yasumoto N, Imai J, Sakamoto H, Tanaka S, Ichikawa S, Ohtani B, Hirai T. Quantum tunneling injection of hot electrons in Au/TiO2 plasmonic photocatalysts. Nanoscale 2017;9:8349–61. https://doi.org/10.1039/c7nr02310c.

[36] Kim J, Son HY, Nam YS. Multilayered plasmonic heterostructure of gold and titania nanoparticles for solar fuel production. Sci Rep 2018;8:1–14. https://doi.org/10.1038/s41598-018-28789-w.

[37] Moon SY, Song HC, Gwag EH, Nedrygailov II, Lee C, Kim JJ, Doh WH, Park JY. Plasmonic hot carrier-driven oxygen evolution reaction on Au nanoparticles/TiO2 nanotube arrays. Nanoscale 2018;10:22180–8. https://doi.org/10.1039/c8nr05144e.

[38] Zhan Z, An J, Zhang H, Hansen RV, Zheng L. Three-dimensional plasmonic photoanodes based on Au-embedded TiO2 structures for enhanced visible-light water splitting. ACS Appl Mater Interfaces 2014;6:1139–44. https://doi.org/10.1021/am404738a.

[39] Pu YC, Wang G, Der Chang K, Ling Y, Lin YK, Fitzmorris BC, Liu CM, Lu X, Tong Y, Zhang JZ, Hsu YJ, Li Y. Au nanostructure-decorated TiO2 nanowires exhibiting photoactivity across entire UV-visible region for photoelectrochemical water splitting. Nano Lett 2013;13:3817–23. https://doi.org/10.1021/nl4018385.

[40] Li H, Li Z, Yu Y, Ma Y, Yang W, Wang F, Yin X, Wang X. Surface-plasmon-resonance-enhanced photoelectrochemical water splitting from Au-Nanoparticle-Decorated 3D TiO2 nanorod architectures. J Phys Chem C 2017;121:12071–9. https://doi.org/10.1021/acs.jpcc.7b03566.

[41] Lu Y, Dong W, Chen Z, Pors A, Wang Z, Bozhevolnyi SI. Gap-plasmon based broadband absorbers for enhanced hot-electron and photocurrent generation. Sci Rep 2016;6:1–9. https://doi.org/10.1038/srep30650.

[42] Peng C, Wang W, Zhang W, Liang Y, Zhuo L. Surface plasmon-driven photoelectrochemical water splitting of TiO 2 nanowires decorated with Ag nanoparticles under visible light illumination. Appl Surf Sci 2017;420:286–95. https://doi.org/10.1016/j.apsusc.2017.05.101.

[43] Fiorenza R, Sciré S, D'Urso L, Compagnini G, Bellardita M, Palmisano L. Efficient H2 production by photocatalytic water splitting under UV or solar light over variously modified TiO2-based catalysts. Int J Hydrogen Energy 2019;44:14796–807. https://doi.org/10.1016/j.ijhydene.2019.04.035.

[44] Yang S, Wang H, Yu H, Zhang S, Fang Y, Zhang S, Peng F. A facile fabrication of hierarchical Ag nanoparticles-decorated N-TiO2 with enhanced photocatalytic hydrogen production under solar light. Int J Hydrogen Energy 2016;41:3446–55. https://doi.org/10.1016/j.ijhydene.2015.12.190.

[45] Sang L, Ge H, Sun B. Probing plasmonic Ag nanoparticles on TiO2 nanotube arrays electrode for efficient solar water splitting. Int J Hydrogen Energy 2019;44:15787–94. https://doi.org/10.1016/j.ijhydene.2018.09.094.

[46] Zhao X, Wang W, Liang Y, Yao L, Fu J, Shi H, Tao C. Three-dimensional plasmonic photoanode of Co3O4 nanosheets coated onto TiO2 nanorod arrays for visible-light-driven water splitting. Int J Hydrogen Energy 2019;44:14561–70. https://doi.org/10.1016/j.ijhydene.2019.04.053.

[47] Sang L, Zhang S, Gao Y. Investigation of plasmonic Cu with controlled diameter over TiO2 photoelectrode for solar-to-hydrogen conversion. Int J Hydrogen Energy 2019;44:25486–94. https://doi.org/10.1016/j.ijhydene.2019.08.047.

[48] Zhou X, Jin B, Luo J, Ning X, Zhan L, Xu X, Fan X, Yang F, Zhang S. One-pot solvothermal synthesis of 1D plasmonic TiO 2 @Ag nanorods with enhanced visible-light photocatalytic performance. Int J Hydrogen Energy 2019;44:10585–92. https://doi.org/10.1016/j.ijhydene.2019.02.234.

[49] Rekeb L, Hamadou L, Kadri A, Benbrahim N, Chainet E. Highly broadband plasmonic Cu film modified Cu2O/TiO2 nanotube arrays for efficient photocatalytic performance. Int J Hydrogen Energy 2019;44:10541–53. https://doi.org/10.1016/j.ijhydene.2019.02.188.

[50] Chaudhary D, Singh S, Vankar VD, Khare N. A ternary Ag/TiO2/CNT photoanode for efficient photoelectrochemical water splitting under visible light irradiation. Int J Hydrogen Energy 2017;42:7826–35. https://doi.org/10.1016/j.ijhydene.2016.12.036.

[51] Liu Y, Gu Y, Yan X, Kang Z, Lu S, Sun Y, Zhang Y. Design of sandwich-structured ZnO/ZnS/Au photoanode for enhanced efficiency of photoelectrochemical water splitting. Nano Res 2015;8:2891–900. https://doi.org/10.1007/s12274-015-0794-y.

[52] Hung SF, Xiao FX, Hsu YY, Suen NT, Bin Yang H, Chen HM, Liu B. Iridium oxide-Assisted plasmon-induced hot carriers: improvement on kinetics and thermodynamics of hot carriers. Adv. Energy Mater. 2016;6:12. https://doi.org/10.1002/aenm.201501339.

[53] Kim H, Choi C, Khamwannah J, Young Noh S, Zhang Y, Seong TY, Jin S. Plasmonic Au nanoparticles on 8 nm TiO2 nanotubes for enhanced photocatalytic water splitting. J Renew Sustain Energy 2013;5. https://doi.org/10.1063/1.4821177.

[54] Mi Y, Wen L, Xu R, Wang Z, Cao D, Fang Y, Lei Y. Constructing a AZO/TiO2 core/shell Nanocone array with uniformly dispersed Au NPs for enhancing photoelectrochemical water splitting. Adv. Energy Mater 2016;6:1501496. /aenm.201501496.

[55] Yildirim DU, Ghobadi A, Soydan MC, Atesal O, Toprak A, Caliskan MD, Ozbay E. Disordered and densely packed ITO nanorods as an excellent lithography-free optical solar reflector metasurface. ACS Photonics 2019;6:1812–22. https://doi.org/10.1021/acsphotonics.9b00636.

[56] Ghobadi A, Dereshgi SA, Hajian H, Birant G, Butun B, Bek A, Ozbay E. 97 percent light absorption in an ultrabroadband frequency range utilizing an ultrathin metal layer: randomly oriented, densely packed dielectric nanowires as an excellent light trapping scaffold. Nanoscale 2017;9:16652–60. https://doi.org/10.1039/c7nr04186a.

[57] Ghobadi A, Yavuz HI, Ulusoy TG, Icli KC, Ozenbas M, Okyay AK. Enhanced performance of nanowire-based all-TiO_2Solar cells using subnanometer-thick Atomic layer deposited ZnO embedded layer. Electrochim Acta 2015;157. https://doi.org/10.1016/j.electacta.2015.01.079.

[58] Ghobadi A, Ghobadi TGU, Karadas F, Ozbay E. Angstrom thick ZnO passivation layer to improve the photoelectrochemical water splitting performance of a TiO2

nanowire photoanode: the role of deposition temperature. Sci Rep 2018;8:16322.

[59] Ghobadi A, Ulusoy TG, Garifullin R, Guler MO, Okyay AK. A heterojunction design of single layer hole tunneling ZnO passivation wrapping around TiO 2 nanowires for superior photocatalytic performance. Sci Rep 2016;6:30587. https://doi.org/10.1038/srep30587.

[60] Lumerical solut. Inc. http://www.lumerical.com/tcad-products/fdtd/., in: Lumerical Solut. Inc. http//www.Lumerical.Com/Tcad-Products/Fdtd/., 2019.